Design and construction of magnetic elements for trapping and transport of cold neutral atoms

Marcius H. T. Extavour

August 2004

Contents

1 Introduction

Since the first experimental realizations of quantum degenerate atomic gases [1, 2, 3, 4] experimental and theoretical interest in the field has exploded. In particular, these landmark achievements in atomic physics have begun to attract attention from the condensed matter physics community. Evidence of the heightened profile of "cold atom" physics can be found in the atomic physics and condensed matter physics literature of proposed and accomplished work in the field: the behaviour of bosonic atoms in periodic potentials formed by optical lattices [5, 6]; quantum phase transitions from

superfluid to Mott insulator states [5, 7, 8]; BEC-BCS crossover physics in ultra-cold molecules [9, 10]; Feshbach resonances in ultra-cold atomic scattering [9, 11, 12, 13, 14]; and novel phases of fermionic atoms in optical lattices [15] are just some of the many rich topics currently under investigation theoretically and experimentally.

Our group is motivated by a desire to probe the fundamental nature of degenerate Fermi gases in order to shed light on outstanding problems in condensed matter physics. These include ground state behaviour of novel magnetic phases, fermion superfluidity and high-T_c superconductivity. Our first step toward this goal is the design and construction of an experimental apparatus to trap and cool neutral fermionic atoms to quantum degenerate temperatures and below.

We began the task of building up our lab in earnest in mid to late 2003. The primary experimental tools required to carry out our ultra-cold gas experiments are 1) stable and frequency-locked laser diodes for laser cooling and for probing and manipulating the atomic ensemble, 2) an ultra-high vacuum chamber capable of reaching pressures of 10^{-9} torr and below, and which also allows optical access to the atomic gas, 3) magnetic field coils and magnetic microtraps to enable the trapping, transport and cooling of the atomic gas, 4) a radio-frequency (RF) source and antenna for evaporative cooling, and 5) an optical imaging system with which to quantify and measure the quantum degenerate gas. My MSc. efforts since September 2003 have focused largely on the magnetic elements of our experiment. My work on the design and implementation of these elements is the focus of this report.

Section 2 of this report describes in greater detail our experimental path from hot classical atomic gas to quantum degenerate gas, outlining the various trapping and cooling stages employed along this path. The following three sections then describe the design, implementation and testing of specific magnetic elements used in our setup. Section 3 is dedicated to the magnetic field coils used to accomplish magnetic trapping of neutral atoms.

Section 4 describes the magnetic microtraps of our "atom chip", a key component in our strategy for trapping and cooing fermions. Section 5 outlines the more technical details of the atom chip-related infrastructure - the "stack" - which supports the atom chip inside the ultra-high vacuum system. Section 6 concludes the report with a summary of work accomplished this year and a note on its relevance to our greater experimental effort.

2 Experimental sequence - trapping and cooling stages

Achieving quantum degeneracy in gases of ultra-cold neutral atoms is a multi-step process. Modern experiments on these systems employ combinations of cooling and trapping techniques developed at different times over the last several decades. The basic elements of our experiment mentioned in the Introduction are combined to enable three successive trapping and cooling stages which transform a hot gas of atoms with temperatures $T \sim 500$ K and phase space densities $\rho \sim 10^{-13}$ into a quantum degenerate gas with $T \leq 10^{-6}$ K and $\rho \sim 10^{5}$. These stages are 1) the magneto-optical trap, 2) the macroscopic magnetic trap and magnetic transport, and 3) the microtrap and evaporative cooling.

Figure 1 is a schematic drawing of the major components of our experimental setup and their relative orientations in the lab. *The indicated coordinate axes are maintained in all figures throughout this report.*

2.1 Magneto-optical trap

In the first of these stages, the magneto-optical trap (MOT), atoms are trapped and cooled from a background vapour inside the vacuum system [16]. Six counter-propagating red-detuned laser beams are directed toward

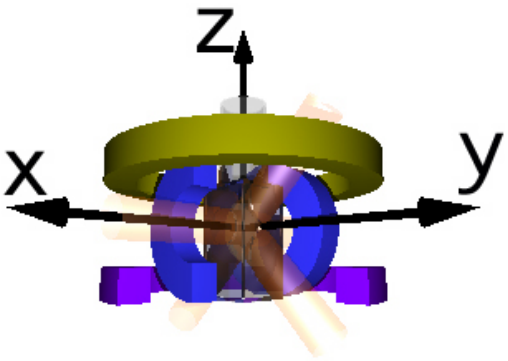

Figure 1: Schematic diagram showing the six counterpropagating laser beams, magnetic field coils used for magneto-optical trapping and magnetic trapping (inner coils) and magnetic transfer (outer coils), the glass vacuum cell, and the defined coordinate axes.

the atomic vapour. A quadrupole magnetic field[1] generated by external field coils is also imposed on the atomic ensemble, having its $B = 0$ centre coinciding with the centre of the laser beam overlap region. Combining the linear magnetic field and laser light in this manner results in a restoring force felt by the neutral atoms directed toward the $B = 0$ centre. This central, linear restoring force defines the MOT, and brings the atoms into the $T \sim$ mK and $\rho \sim 10^{-6}$ regime.

2.2 Magnetic trap and transfer

Once trapped in a MOT the atoms are then loaded into a purely magnetic trap. This trap consists single quadrupole field having a linear field gradient much larger than that of the MOT quadrupole field. In our experiment the same pair of coils used in the MOT also generate the much larger field of the magnetic trap. As explained in Section 2.4, in this trap the magnetic dipole

[1]A quadrupole magnetic field is a field in which the magnitude $|\vec{B}|$ increases linearly in all directions from a central $|\vec{B}| = 0$ point.

moments of atoms in certain magnetic hyperfine states interact with the external magnetic field in such a way that their potential energy is minimized at the $B = 0$ minimum of the field. This potential minimum results in strong confinement of the neutral atoms. By applying a separate, uniform magnetic field to the trapped atoms their position in space is shifted through several centimetres toward the stationary atom chip. Once near the chip's surface the atoms are loaded from the macroscopic trap into the magnetic microtrap. There the atoms are evaporatively cooled to quantum degeneracy and are confined while probed or manipulated as part of a given experiment.

2.3 Atom chip and evaporative cooling

The atom chip consists of microstructured conductors on a planar, insulating substrate. The combination of current-induced static magnetic fields from these microstructures and external uniform magnetic fields allow the realization of tiny (tens of micrometres) magnetic traps tens or hundreds of micrometres from the chip surface. These microtraps are similar in principle to the macroscopic magnetic trap described in Section 2.2, but have trap gradients orders of magnitude larger. The large gradients are required for efficient evaporative cooling of the cold atoms.

Using RF radiation of the appropriate frequency it is possible to induce transitions to untrapped magnetic hyperfine states in only a certain velocity class of atoms. By forcing only the hottest (largest-velocity) atoms from the trap[2] the system will eventually rethermalize via atomic elastic collisions to a reach a new equilibrium in which the mean temperature of the atoms is lower than its original value. Applying this forced RF evaporation procedure repeatedly allows the atomic sample's temperature to be reduced and phase-space density increased to the point of quantum degeneracy. This represents the end of the gas cooling stage, and also the point at which exper-

[2]Once an atom makes a transition to a magnetically-untrapped hyperfine state it will quickly be repelled from the trap.

iments meant to probe the nature of the quantum degenerate atoms begin. sectionMagneto-optical trap and macroscopic magnetic trap The magneto-optical trap (MOT) and magnetic traps are key ingredients in our procedure for cooling and trapping neutral atoms. Since these elements of our experiment will likely be present in all future studies of Fermi or Bose physics it was important to implement a reliable and efficient design for both systems.

The basic design challenges were as follows. For the MOT we required a three-dimensional quadrupole magnetic field to work in conjunction with six counterpropagating laser cooling beams. The pure magnetic trap required a similar magnetic field configuration, but with a field gradient roughly one order of magnitude larger than that required for the MOT. These two field constraints needed to be satisfied in such a way that the appropriate magnetic fields and magnetic field gradients could be generated in the region of the glass vacuum cell without overly restricting the optical access to the cell.[3]

The design and implementation of the MOT and magnetic field geometries was a process of 1) analytic field calculation, 2) selecting an appropriate coil geometry, 3) fabricating the coils themselves and 4) quantifying the results with field measurements and actual tests on cold atoms. The design constraints and final solution are described individually below, as is some of the physics relevant to the magnetic trapping of neutral atoms.

2.4 Physics of the magnetic trap

2.4.1 A confining potential

The confinement of neutral atoms by magnetic field minima is neatly described by potential energy arguments.

The potential energy of an atom with magnetic dipole moment $\vec{\mu}$ in an

[3]Optical access in this case means clear paths for the cooling laser beams as well as the imaging system(s) and probe laser beam(s).

external magnetic field $\vec{B}$ is given by

$$U = -\vec{\mu} \cdot \vec{B} \tag{1}$$

For an atom in the magnetic hyperfine level characterized by m_F the energy can be rewritten as

$$U = g_F m_F \mu_B B \tag{2}$$

where g_F is the Landé g factor for the given hyperfine level[4] and μ_B the Bohr magneton [18]. From this expression it is clear that the potential energy U is directly related to the magnetic field strength B. A quadrupole magnetic field, in which the magnitude grows linearly in all directions from a single $B = 0$ point, thus corresponds to a confining or "trapping" potential for the atom.

2.4.2 Weak-field seekers

Examining equation (2) and noting that B and μ_B are positive quantities, it follows that the product $g_F m_F$ must be positive for a potential minimum to correspond to a magnetic field minimum.[5] The sign of $g_F m_F$ depends on the particular hyperfine state occupied by the atom. In particular, it is a function of the atomic angular momentum quantum numbers F, J, I, L and S [16]:

$$g_F = \left[1 + \frac{J(J+1) + S(S+1) - L(L+1)}{2J(J+1)}\right]\left[\frac{F(F+1) + J(J+1) - I(I+1)}{2F(F+1)}\right] \tag{3}$$

S, L and I are the electron spin angular momentum, orbital angular momentum and nuclear spin angular momentum quantum numbers respectively.

[4] F is the total angular momentum quantum number and $-F \leq m_F \leq F$ as usual.

[5] The very existence of magnetic field maxima in free space are ruled out by Maxwell's equations [17].

$J = L + S$ and $F = J + I$. Those states having $g_F m_F > 0$ are referred to as *weak-field seekers* and can be confined by a magnetic field minimum. On the other hand, atomic states having $g_F m_F < 0$ are termed *strong-field seekers* and are repelled from magnetic field minima. An efficient magnetic trap therefore relies on the atoms being in weak-field seeking or "trappable" states. In the case of ^{40}K, for instance, the $|F = 9/2, m_F = 9/2\rangle$ sub-level of the $4S_{1/2}$ ground state is a trappable candidates since it has $g_F m_F = \frac{2}{9}\frac{9}{2} = +1$.

2.5 Design parameters

Having settled on the idea of trapping atoms in a quadrupole field configuration, the next step was to identify physical and technical constraints and to make quantitative estimates before exploring coil designs.

2.5.1 The effect of gravity on magnetically trapped atoms

A cold atom in a quadrupole trap feels a force acting on its magnetic moment in the presence of the magnetic field gradient. There is another force relevant to the trap, however, and that is the force of gravity acting on the mass of each atom. Thus in order to effectively confine atoms to a particular region of space it is important to compute the value of the gravitational force.

The force of gravity acting on a single ^{40}K is $F = mg$. To prevent the atom from accelerating toward the earth this force must be balanced by an upward force provided by the magnetic field. $F = -\nabla U$ for a conservative potential U. Combining this with equation (2) results in a second force equation $F = -\nabla U = g_F m_F \mu_B \frac{dB}{dz}$. Setting these two forces equal results in an estimate of the trapping magnetic field gradient needed to overcome the downward pull of gravity. Using the fact that $g_F m_F = \frac{2}{9}\frac{9}{2} = 1$ for the $|F = 9/2, m_F = 9/2\rangle$ state and setting the two force equations equal yields $\frac{dB}{dz} \doteq 7$ G/cm. This result means that any usable magnetic trap for ^{40}K atoms must have a magnetic field gradient of at least 7 G/cm, which is a very useful lower

bound to be aware of. The corresponding value for ^{87}Rb atoms in the $|F = 2, m_F = 2\rangle$ level of the ground state is 15 G/cm.

2.5.2 Magnetic transfer distance

As described in detail in the next sections, our experiment relies on the transport of magnetically trapped atoms through a distance of some centimetres. This transfer does not improve the trapping and cooling process in any way, but is rather a necessity of our experimental approach.

A lower bound on the actual distance of this transfer was fixed by the size of our atom chip and the diameter of the trapping laser beams, as shown in Figure 2.

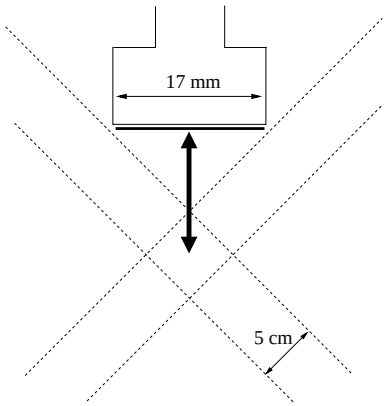

Figure 2: The atom chip (thick horizontal line) sits just below the end of its support block. MOT beams (dashed lines) pass as near as possible to the chip without clipping it. The diameter of the beams and the width of the chip thus fix a minimum transfer distance in this geometry of 4.39 cm, shown above with the vertical two-way arrow.

The beams are aligned at right angles for optimal capture efficiency in the MOT. In the interest of keeping scattered light to a minimum the atom chip needed to be positioned outside of the beam diameters. This fact, along with the width of the atom chip itself and the laser beam diameter sets a

minimum separation between the centre of the beams (the site of the MOT) and the surface of the chip (see Fig.2).

2.5.3 Glass cell diameter and MOT coil separation

The ultra-cold atoms in our experiment are manipulated inside an evacuated glass cell. The cell has the shape of a square prism whose dimensions were chosen to accommodate our 5 cm diameter trapping laser beams. The cell size of 7.5 cm (the width of each face) thus sets a lower bound on the possible separation of magnetic field coils positioned outside of the cell. The minimum separation also affects the the final coil radius since it is desirable to keep the MOT coil geometry close to the anti-Helmholtz geometry[6] to maximize the quadrupole field gradient generated per amp of DC current.

2.5.4 Fast magnetic field switching

Loading atoms from one trapping potential to another requires fine control over the turn-on and turn-off of the individual traps. Fast switching of magnetic field coils presents a particular challenge because of the oscillatory nature of current and voltage in LRC circuits (a field coil is nothing more than a large inductor and small resistor). As such, it was important to minimize inductance in the final coil system to allow the large currents eventually required to be electronically switched with time constants $\tau \sim 100$ μs and lower.[7]

2.6 Analytics of circular coil B fields

In order to design appropriate magnetic fields for the MOT and quadrupole traps it was necessary to have a reliable way of computing magnetic vector fields produced by a given arrangement of conductors. In designing the

[6] Coil radius $\approx$ coil separation

[7] 100 μs is an approximate value based the experience of other research groups and literature.

dual-function MOT and magnetic trap coils it was clear that circular coil geometries were by far the simplest way to achieve the desired fields, both in terms of coil fabrication and field calculation. Further, since we transfer atoms to a final magnetic microtrap to reach quantum degeneracy, the magnetic traps arising from simple circular current geometries are more than sufficient.

Analytic expressions for the vector field $\vec{B}$ from realistic coil geometries were developed and used extensively in *Mathematica* to evaluate coil designs. The engines of this code are the analytic expression for the radial and axial components of an infinitely thin circular wire in terms of elliptic integrals:

$$B_r = \frac{\mu I}{2\pi r}\frac{z-A}{[(R+r)^2+(z-A)^2]^{1/2}}\left[-K(k^2)+\frac{R^2+r^2+(z-A)^2}{(R-r)^2+(z-A)^2}E(k^2)\right] \quad (4)$$

$$B_z = \frac{\mu I}{2\pi}\frac{z-A}{[(R+r)^2+(z-A)^2]^{1/2}}\left[K(k^2)+\frac{R^2-r^2-(z-A)^2}{(R-r)^2+(z-A)^2}E(k^2)\right] \quad (5)$$

$$k^2 \equiv \frac{4Rr}{(R+r)^2+(z-A)^2}, \quad (6)$$

where R is the loop radius, A the location of its centre on the z axis, r and z the radial and axial coordinates, and K and E the complete elliptic integrals [20, 21]. By summing the fields produced by many such single loops each slightly displaced from one another the total magnetic field of a realistic circular coil could be well estimated.

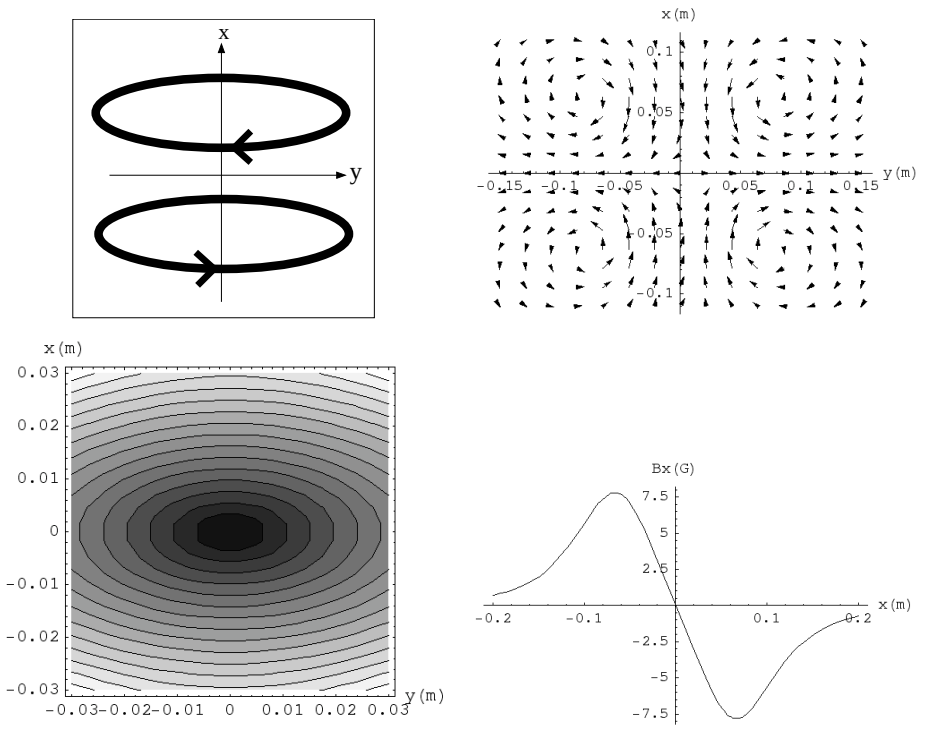

Figure 3: Calculated magnetic fields generated by anti-Helmholtz coils. Upper left: orientation and current direction of the coils. Upper right: in-plane vector field. The quadrupole trap is centred at the origin. Lower left: a contour plot of the central quadrupole trap region. Lower right: z-component of the magnetic field along the x asis, showing the linearity of the field near the origin.

It is worth pointing out here that, strictly speaking, the above analytic expressions give only *two* spatial components of the field - axial (x) and radial (y, z). In the case of a radially symmetric current loop, however (e.g. a circular loop), these two components fully characterize the 3D field since all radial spatial dimensions are degenerate. In other words, the 2D vector fields which were actually computed could be extended to 3D by taking advantage of the basic symmetry of the problem.

The validity of the $\vec{B}$ calculations was confirmed with measurements on a real coil. Computed and experimentally measured[8] magnetic field magnitudes along the axial direction of a single circular coil are shown in Figure 4.

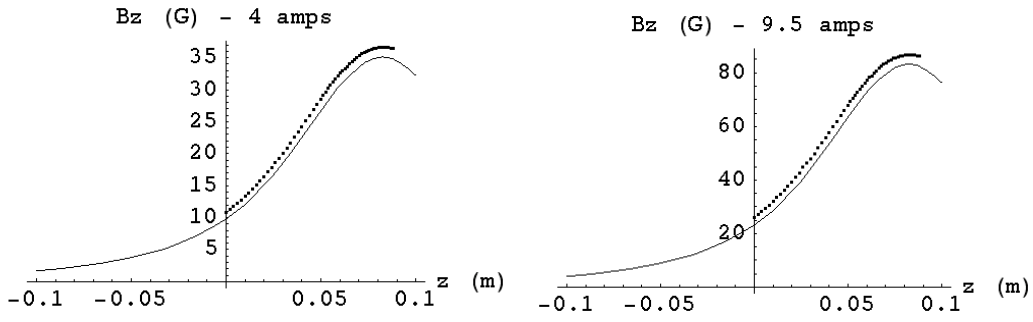

Figure 4: Calculated (solid line) and measured (dots) magnetic fields produced by a single MOT coil; 100 turns, 5 cm inner radius. The left plot shows data collected with a DC current if 4.5 A in the coil, the right, 9 A.

Inspection of these figures reveals an error of roughly 5% between the calculated and measured field values. Although the error appears to be systematic, it is small enough that any calculated field estimates may be trusted for the purposes of preliminary design. After final construction the coil fields were more carefully measured to within a measurement error of $\sim 2\%$.

[8]The magnetic field values were measured at constant DC current in the coil with a gaussmeter probe mounted on a translation stage.

2.7 Final coil design: the off-centre MOT and magnetic transfer

This section describes the design chosen to meet all of the design criteria within the design constraints. The section concludes with a table summarizing the final coil parameters and operating points.

In our approach to cooling and trapping neutral atoms we begin by collecting atoms in a large MOT 5 cm away from the atom chip and subsequently load them into a macroscopic magnetic trap[9] at the same site. The magnetically trapped atoms are then magnetically transferred to the surface of the atom chip. Finally the atoms are loaded from this macroscopic trap into the magnetic microtrap.

The various stages of this approach required a system of magnetic coils which could produce the magnetic fields necessary for the MOT, macroscopic magnetic trap and the transfer of the trapped atoms through a 5 cm distance. The chosen geometry and trapping sequence meet all of the design criteria without compromising the optical access of the system and while dissipating as little power as possible.

2.7.1 Coil geometry details

The MOT, magnetic trap and transfer are carried with four coils (two pairs) artistically depicted in Figure 5. The inner pair of coils - the "MOT coils" - create the linear quadrupole fields for the MOT and magnetic trap. They consist of 100 turns of insulated, hollow-core[10] copper wire and have inner diameters of 10 cm and outer diameters of 18.4 cm. Their inner separation is 8.4 cm. The MOT is achieved by passing equal but opposite 5.94 A DC cur-

[9]This macroscopic trap is generated by large, external field coils rather than the microscopic lithographic conductors of the atom chip.

[10]The wire is hollow to allow the flow of pressurized cooling water through the centre of the wire.

rents through each coil.[11] The outer coils - the "transfer coils" - carry equal parallel currents and thus provide a nearly uniform field in the z direction. They are made of the same hollow-core copper wire, but have 49 turns each, have inner diameters of 28 cm and outer diameters of 36.4 cm. Their inner separation is 11.4 cm. Applying this uniform field to the quadrupole field of the MOT coils shifts the location of the $B = 0$ trap centre by exactly 2.5 cm. Varying the current in the transfer coils (and hence the field strength) while keeping that of the MOT coils fixed thus allows the trap centre to be repositioned along the z axis. The MOT laser beams are aligned so that they intersect at this same $z = -2.5$ cm spot on the z axis.[12]

Figure 5: The full experimental setup. This image shows the position of the MOT (central sphere) as well as the MOT and transfer coils, glass vacuum cell, MOT beams and atom chip.

Once the cooled atoms are ready to be loaded into the magnetic trap the beams are shut off and the currents in the MOT and transfer coils are

[11] Coils bearing opposing currents are often loosely called *anti-Helmholtz* coils, be they in the Helmholtz geometry or not.

[12] See Fig.1 for a definition of the coordinate axes. The geometric centre of the pair of MOT coils coincides with the origin.

simultaneously ramped up to 65 A and 42 A respectively over several hundred microseconds. The increase of current in the MOT coils creates a quadrupole trap a field gradient of 100 G/cm along the x direction and 50 G/cm along y and z. The commensurate field increase in the transfer coils is needed to maintain the magnetic trap centre at $z = -2.5$ cm.[13]

With the atoms held in the magnetic trap at $z = -2.5$ cm the next step is to transport them up to just below the surface of the atom chip, which is located at $z = +2.5$ cm. This transfer is carried out by adiabatically reversing the direction of the transfer bias field produced by the transfer coils. This shifts the cold atoms from $z = -2.5$ cm to $z = +2.5$ cm. Reversing the bias field direction simply repositions the $B = 0$ centre of the quadrupole trap to just beneath the surface of the atom chip.

2.8 Advantages and caveats

The most significant advantage of this off-centre MOT setup is its power efficiency. The off-centre MOT saves over an order of magnitude of power as compared to a setup based on a conventional centred MOT. The reasons for this power efficiency are described here.

Analytic calculations of the quadrupole field showed that the magnetic trap formed in the centre could indeed by shifted by applying a uniform bias field, but only to a certain distance. The trap centre can be shifted out to $z = \pm R/2$, where R is the coil radius, without sacrificing trap depth or field gradient. Beyond this point, the quadrupole trap was seen to degrade: decreasing trap depth and field non-linearity set in at $|z| > R/2$.

Given the constraints on the maximum possible magnetic transfer distance $R/2$ and the minimum required transfer distance d, we might have tried setting the coil MOT radius equal to twice the desired transfer distance: $R/2 = d$. In such an arrangement the MOT and magnetic trap would be

[13]The value of the uniform field required to offset the trap centre by a given distance depends directly on the value of the linear field *gradient*.

located at the centre of two quadrupole coils and could be safely transferred vertically to $z = \pm R/2$. The coil size and power dissipated is considerably reduced, however, if the MOT and magnetic trap are positioned *off-centre* with respect to the MOT coils - specifically at $z = -R/4$. Under this scheme, which is the one adopted in our experiment, atoms move from below to above centre of the MOT coils and the MOT coil radius R is equal to the transfer distance d. This allows the coils themselves to be *one half the size* and thus to dissipate *one sixteenth* the power compared with coils having $R/2 = d$.[14] As an additional advantage, the net inductance of the MOT coils is greatly reduced by reducing their size and current, which enables much easier and faster switching of large DC currents.

One downside of this approach is that the transfer coils are required to be on at all times; they shift the trap centre downward for the MOT and then upward to load the atom chip. This means that the MOT and transfer coils, which bear separate and independent currents, must be switched as close to simultaneously as possible. Asynchronous switching of these coils would likely add unwanted momentum to the trapped atoms and thus lead to heating. Extra care is being taken with the high-power electronic switch in order to address this potential problem.

Table 1 lists important coil parameters and operating points for the MOT and transfer coils. The completed coils themselves are visible in Figure 13.

3 The atom chip magnetic trap

The final stage of our trapping and cooling of neutral atoms involves loading the atoms into a magnetic microtrap. This microtrap consists of a magnetic

[14]For a circular coil, $P \sim I^2$, $I \sim r^2$ and $B \sim I/r^2$, where P, I, R, r and B represent electrical power, current, resistance, coil radius and magnetic field amplitude. For a fixed magnetic field B, halving the coil radius means the current must be decreased by a factor of four. A factor of four decrease in current in turn implies a factor of 16 decrease in the dissipated DC power.

	I.D.	O.D.	N	sep'n	I_{MOT}	$I_{M.T.}$	R	L
MOT	10 cm	18.4 cm	100	8.4 cm	5.94 A	65 A	0.10 Ω	2.3 mH
X-FER	28 cm	36.4 cm	49	11.4 cm	2.89 A	42 A	0.11 Ω	2.8 mH

Table 1: MOT and transfer coil design parameters and operating points. The column headings are, from left to right, inner diameter (cm), outer diameter (cm), number of turns, inner separation, MOT operating current, magnetic trap operating current, resistance and inductance. The MOT coils generate 1.56 G/cm of linear field gradient near their centre per amp of DC current. The transfer coils generate a uniform field near their centre of 3.03 G per amp of DC current.

field minimum similar to that produced with the MOT coils, but rather is achieved using microscopic lithographic conductors on a planar insulating substrate. This "atom chip" - i.e. the substrate and conductor structure - is suspended inside the vacuum chamber 5 cm above the location of the MOT.

This section opens with an overview of the advantages and disadvantages of trapping neutral atoms in magnetic microtraps. Next, the formation of magnetic field minima with planar conductors and uniform bias fields is introduced. Subsequent subsections summarize analytic and numerical calculations of magnetic field offsets, gradients, and curvatures achievable in U and Z traps. The section closes with a description of our current atom chip, the Orsay chip.

3.1 Motivation for atom chip approach

Magnetic microtrap experiments offer several key advantages over traditional cold atom experiments, but are also limited in several respects. The physical advantages and disadvantages of the microtrap approach are summarized here.

First, the miniaturization of the magnetic field sources (the wires, in this case) results in much larger magnetic fields, field gradients and field

curvatures for a given electric current. This allows, for instance, T/cm field gradients with currents as low as one or two amps, in stark contrast to the hundreds of amps required to achieve similar gradients in large field coils. Further, bringing atoms very near to such microstructures allows these benefits to be put to good use in tightly confining the atoms. (Recall that $B(r) = \frac{\mu_0 I}{2\pi r}$ with distance r from an infinite wire.)

Extremely strong confinement of atoms in these microtraps can enhance the elastic collision rate between atoms by factors of 10 or 20. Since these collisions drive re-thermalization during evaporative cooling, microtraps can afford one- or two- second evaporation times, rather than tens of seconds or even minutes as in many conventional magnetic traps [22]. This increased confinement typically comes at the expense of trap depth, however, which is the main detraction of the chip trap approach. The atom number in many chip trap experiments is limited to between 10^3 and 10^6 atoms, compared to clouds of 10^7 or 10^8 atoms achievable in conventional macroscopic magnetic traps [18]. Experiments requiring higher atom numbers, such as vortex experiments in BECs, may thus be out of reach of current microtraps.

The enhanced confinement and reduced evaporation time in turn ease the constraint on the magnetic trap lifetime. Magnetic trap lifetime is typically determined by the rate of collisions between cold trapped atoms and hot background particles. Strong confinement and short evaporation times mean that chip trap experiments can withstand much higher background pressures in the vacuum chamber since the atoms need not be trapped for nearly as long a time. Practically, a chip trap experiment may operate with a vacuum pressure one or two orders of magnitude higher ("worse") than a conventional experiment, which is a significant advantage.

Finally, in terms of the experimental physics available to atom chips, there are many possibilities such as one-dimensional traps, trap-to-trap tunnelling, coherent guiding and splitting of condensates and transportation of condensates which are technically impractical or impossible with conventional field

coil experiments. As such, chip traps can provide access to genuinely new physics, in addition to their other technical advantages.

3.2 U and Z magnetic microtraps

Many magnetic field geometries traditionally generated with coils can be replicated by planar conductor patterns and uniform bias fields [18, 23, 24]. Our atom chip contains two such configurations, referred to here as "U" and "Z" traps. These wire traps are manifestations of quadrupole (linear) and Ioffe-Pritchard (quadratic) magnetic traps for neutral atoms.

To understand the trapping action of these wire traps it is useful to first consider the simple case of a single wire and perpendicular bias field. A straight and infinite wire carrying current along its length produces magnetic field circulating about the wire.

If an external uniform magnetic field is introduced in a direction perpendicular to the wire, a magnetic field zero is generated at some fixed distance above the wire (see Figure 6). This magnetic field minimum constitutes a quadrupole magnetic trap; the trap is confining in two dimensions only and runs to positive and negative infinity at a fixed height above the wire. A usable magnetic trap for our purposes, however, must be confining in all three spatial dimensions. The next section describes the added confinement employed in U and Z traps and the resulting differences in their magnetic field minima.

3.3 U and Z trap analytics

Full three-dimensional confinement of atoms requires the addition of some magnetic confinement along the free dimension of the aforementioned wire trap. The U and Z traps are distinguished in the way in which they provide this extra confinement and in the resulting magnetic field minima.

The U trap is formed by truncating this infinite wire and terminating it

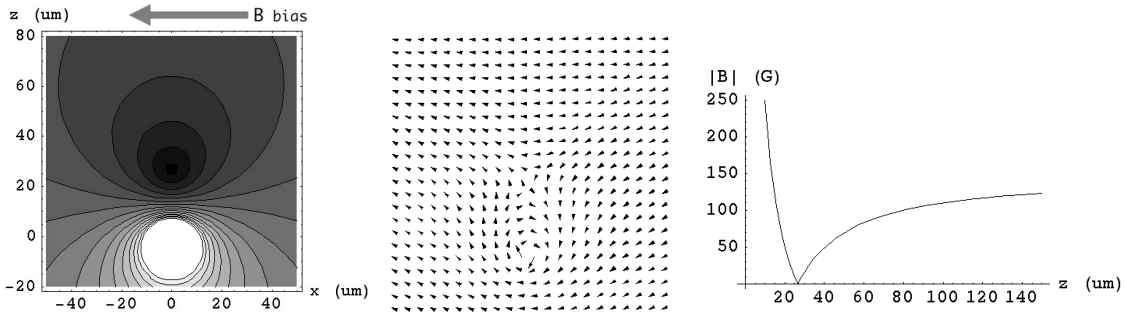

Figure 6: The above plots depict the net magnetic field produced by an infinite, straight current-carrying wire and a uniform perpendicular bias field. The wire bears current *into* the plane of this page, intersecting the xz plane at the origin. The direction of the external bias field is indicated in the left figure, which also shows a contour plot of the net field magnitude in the plane. The dark circle at $z \sim 27$ μm represents the $B = 0$ trap centre. The centre plot shows the net magnetic vector field. The range an axes in this plot are identical to those in the contour plot, but were omitted for the sake of clarity. The right figure shows the magnetic field amplitude along the z axis. Notice the magnetic field minimum at $z \sim 27$ μm. All the above figures were computed using a wire current of 2 A and a bias field of 150 G.

with two parallel wire segments as shown in Figure 7. The Z trap is also formed by truncating the infinite wire, but in such a way that the three segments form a Z pattern (Fig.7). Current flows through all three segments of the U or Z wires equally. When the magnetic field vectors of each segment are added to the uniform bias field, a tube shaped three-dimensional magnetic field minimum emerges. In the case of the U trap, this field is a quadrupole field, where the field intensity increases linearly in all directions from the $B = 0$ trap centre. In the case of the Z trap, the minimum can be classified as a Ioffe-Pritchard harmonic trap since the magnetic field increases quadratically in one direction from the $B \neq 0$ trap centre.

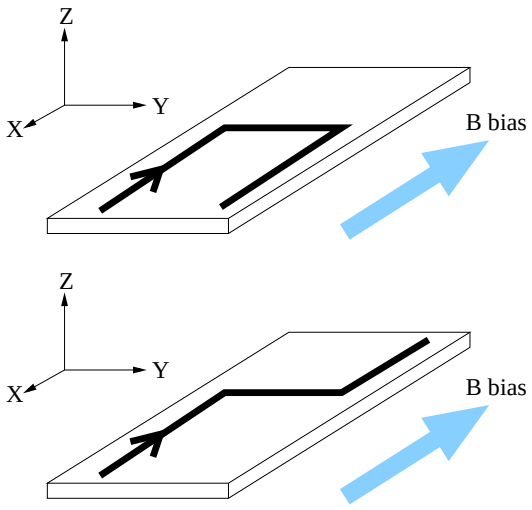

Figure 7: Schematic diagrams of the U (upper) and Z (lower) wire trap configurations. The arrows on the chip surfaces indicate the flow of DC current.

3.4 Strong trap axes

The x and z axes of both traps are termed the "strong axes" since magnetic confinement (the magnetic field gradient) is strongest along this direction. The weak axis is the y axis for both U and Z traps. Analytic magnetic field calculations are simplest along the strong axis. This is due to the fact that in determining strong axis gradients and curvatures near the centre of the trap one may neglect the magnetic field contributions of the terminating wires and simply assume the magnetic field behaviour of an infinite wire segment.[15]

The magnetic field, gradient and curvature in the x direction can thus easily expressed to a very good approximation as

$$B_x(x) \quad = \quad \frac{\mu_0}{2\pi}\frac{I}{x} - B_{bias} \tag{7}$$

[15]Note that only the central wire segment and the external bias contribute to the x-component of the net microtrap magnetic field.

$$\frac{dB_x(x)}{dx} = -\frac{\mu_0}{2\pi}\frac{I}{x^2} \quad (8)$$

$$\frac{d^2B_x(x)}{dx^2} = \frac{\mu_0}{\pi}\frac{I}{x^3} \quad (9)$$

The derivation of the equivalent expressions along the weakly-confining y axes is outlined in the next section.

3.5 Weak trap axes

The terminating wire segments of the U and Z traps contribute to the y-component of the net magnetic field since they generate fields in the yz plane only. The two terminating segments bear current in equal directions in the case of the Z trap, and in opposite directions in the U trap. Nevertheless, the general procedure for combining the y-component fields is the same in both cases and both are described together below.

$B_y(y)$ must first be determined since from this quantity the field offset $B_y(0)$, gradient $\frac{dB_y(y)}{dy}|_{y=0}$ and curvature $\frac{d^2B_y(y)}{dy^2}|_{y=0}$ may be derived. Since the magnetic field minima in both U and Z traps occur away from the surface of the atom chip (the xy plane) the calculation will be carried out for a trap at an arbitrary distance z_0 from the chip surface.

Figure 8 shows the fields generated in the yz plane by the two terminating wire segments of the U and Z traps. The length of the central wire segment along the y axis is set arbitrarily to $2L$. The two diagrams differ by the fact that the terminating wires bear currents in different directions depending on the trap type. Following the diagrams the y components of the U and Z traps along $x = 0$ can be written down as

$$B_y^U(y) = \frac{\mu_0 I}{2\pi r_1}\frac{z_0}{r_1} - \frac{\mu_0 I}{2\pi r_2}\frac{z_0}{r_2} \quad (10)$$

$$B_y^Z(y) = \frac{\mu_0 I}{2\pi r_1}\frac{z_0}{r_1} + \frac{\mu_0 I}{2\pi r_2}\frac{z_0}{r_2} \quad (11)$$

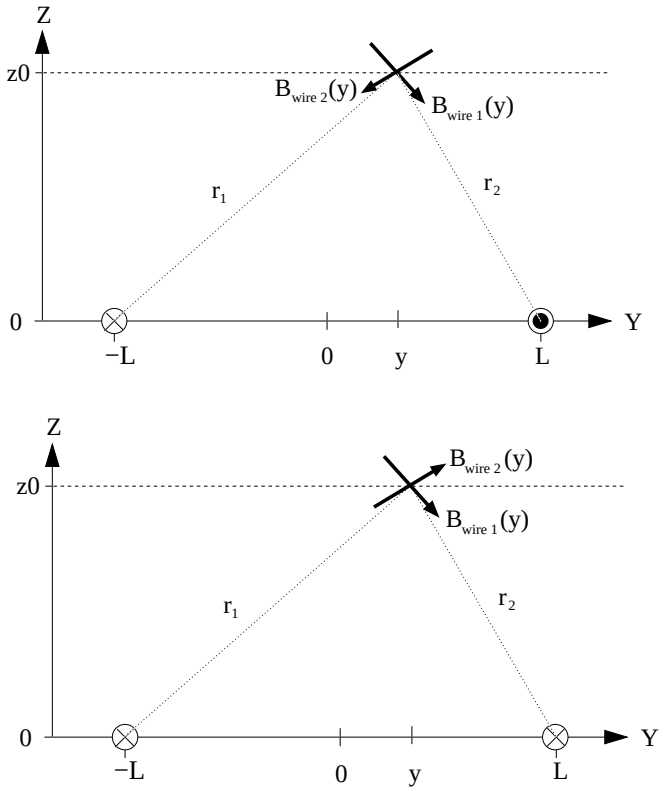

Figure 8: These diagrams show schematically the magnetic fields generated in the yz plane by terminating wire segments of the U and Z traps. r_1 and r_2 are the the distances in the plane from the left and right terminating wires respectively to a point ($Y = y$, $Z = z_0$) away from the surface of the chip.

Using the geometric relations $r_1^2 = z_0^2 + (L-y)^2$ and $r_2^2 = z_0^2 + (L+y)^2$ (see Fig.8) above expressions reduce to

$$B_y^U(y) = \frac{\mu_0 I z_0}{2\pi}\left[\frac{1}{z_0^2+(L-y)^2} - \frac{1}{z_0^2+(L+y)^2}\right] \quad (12)$$

$$B_y^Z(y) = \frac{\mu_0 I z_0}{2\pi}\left[\frac{1}{z_0^2+(L-y)^2} + \frac{1}{z_0^2+(L+y)^2}\right] \quad (13)$$

The field offset, gradient and curvature near the trap centre ($y \ll L$) are now easily obtained from these expressions. For the U trap

$$B_{offset} = B_y^U(0) = 0 \quad (14)$$

$$B_y'(y \to 0) = -\frac{2\mu_0 I}{\pi L^3} \quad (15)$$

$$B_y''(0) = 0 \quad (16)$$

where $z0 \ll L$ and $y \ll L$ have been assumed.[16] Note that the U trap has zero offset field, a uniform gradient and zero curvature at the trap centre, confirming that it is indeed a quadrupole magnetic trap. For the Z trap

$$B_{offset} = B_y^Z(0) = \frac{\mu_0 I}{\pi}\frac{z_0}{z_0^2+L^2} \quad (17)$$

$$B_y'(y \to 0) = 0 \quad (18)$$

$$B_y''(0) = \frac{6\mu_0 I z_0}{L^4}\frac{1 - z_0^2/3L^2}{(1+z_0^2/L^2)^3} \quad (19)$$

The Z trap has a non-zero offset, zero gradient and a uniform curvature at the trap centre, confirming that it is a Ioffe-Pritchard-type harmonic trap.

Table 2 lists calculated U and Z trap parameters of the Orsay microchip (see Section **??**) under normal operating conditions.

[16] Typical values of z_0 and L for the Orsay chip are 27 μm and 2 mm. The assumption is a good one.

Trap	I	B_{bias}	B_{offset}	$B'_{x,z}(0)$	$B'_y(0)$	$B''_y(0)$	L	z_0
U	2 A	150 G	0	6.6 T/cm	14.6 G/cm	0	1.03 mm	27 μm
Z	2 A	150 G	0.03 G	6.8 T/cm	0	96.12 G/cm^2	1.44 mm	27 μm

Table 2: A summary of realistic operating parameters for the U and Z microtraps.

3.6 Limits to analytics

The analytic expressions of the previous section are only valid near the trap centre $x = 0, y = 0$. Trap quantities which require information about the entire trap field, such as the trap depth, must therefore be computed by other means. Figure 9 shows contour plots parallel to the xy plane of the full magnetic minima generated in U and Z traps. The fields were computed following the Biot-Savart formula for the magnetic field produced by *finite* current-carrying wire segments. These Biot-Savart calculations are also a good check of the analytic expressions.

3.7 Magnetic minima and Majorana loss

This section gives qualitative descriptions of the U and Z trap magnetic field minima and explains why that of the Z trap is best suited for trapping cold atoms.

As mentioned above, the U field configuration corresponds to a quadrupole magnetic trap and the Z to a harmonic trap. The zero crossing (sign change) of the magnetic vector field at the centre of the U trap, however, renders the trap susceptible to Majorana "spin flip" losses, as is the case with all quadrupole magnetic traps. The Majorana loss process is easily described within a classical framework. Classically, the atomic magnetic moment precesses about the direction of the magnetic field vector at a rate given by the classical Larmour frequency. This spin moment may adiabatically follow a spatially varying magnetic field provided that the rate of change of the *di-*

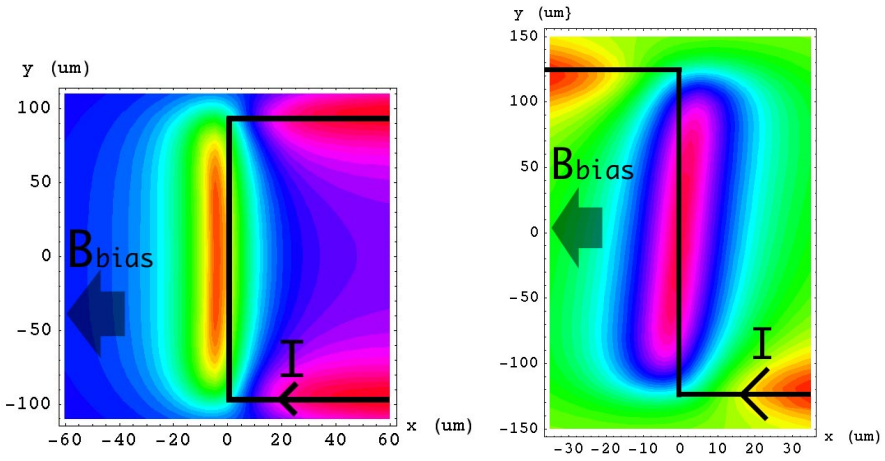

Figure 9: Contour plots showing the magnetic field intensities produced by the U and Z wires and indicated bias magnetic fields in a plane parallel to the atom chip surface. The black line shows the position of the wires relative to the field minimum.

rection of the magnetic field vector does not exceed the Larmour frequency. Since there is a zero crossing at the centre of a quadrupole trap, any atom passing through this centre will maintain its spin orientation to a large degree and, in failing to adiabatically follow the rapidly changing magnetic field, be lost from the trap. This process is generally referred to as Majorana loss.

The Z trap avoids this problem since the magnetic field offset is nonzero and the magnetic minimum contains no zero crossing of the magnetic field. The harmonic trapping potential of the Z trap is therefore the preferred microtrap for our experiments. The U trap, while not suitable for trapping the coldest atoms due to Majorana loss, is still valuable as a temporary chip trap for atoms en route from the macroscopic magnetic trap to the final Z trap.

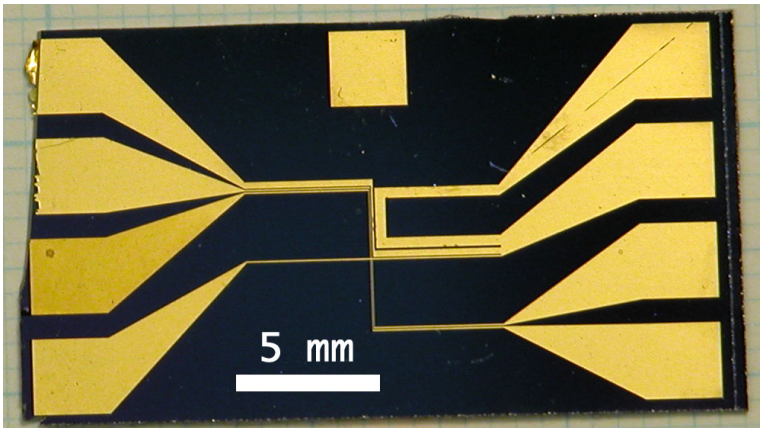

Figure 10: Top view of the Orsay chip. Gold conductors were deposited onto a Si substrate via photolithography and electroplating techniques.

3.8 The Orsay atom chip

Our current atom chip consists of microfabricated gold wires on a SiO_2-coated substrate. The substrate is a cleaved section of a single crystal epitaxial Si wafer. Its length, width and thickness are roughly 16 mm, 28 mm and 200 μm. The gold wires and contact pads were added to the substrate using photolithography and electroplating. The wires have rectangular cross-sections, with thicknesses ranging from 20 to 460 μm and heights of 7 μm.

Our atom chip was a gracious donation from the Groupe D'Optique Atomique of Alain Aspect at l'Institut d'Optique in Orsay, France. The gift of one of their spare chips allows us to experiment with the loading of microtraps while we pursue the design and fabrication of our own first-generation atom chips.

4 Stack design and fabrication

The "stack" is the name given to the supporting infrastructure of the atom chip in the vacuum chamber. This stack performs three key functions: first,

it provides a physical platform upon which to attach the atom chip; second, it provides a convenient scaffold around which to build electrical connections to the atom chip; third, it heatsinks the atom chip. This section will describe the design process used in making our current stack and describe the completed stack.

4.1 Stack body

Oxygen-free high conductivity (OFHC) copper was chosen as a base material for the stack because of its UHV compatibility, machinability and excellent thermal conductivity. This third feature of OFHC copper (and copper in general) is meant to allow excessive heat generated at the chip wires to be dissipated as efficiently as possible.

The body of the stack consists of machined copper pieces held together by stainless steel screws. At one end the stack is affixed to the vacuum side of a 6" UHV stainless steel flange. The other end of the stack is a T-shaped solid copper block to which the chip is affixed.

4.2 Attaching the chip

The chip is attached to the stack by means of home-made macor[17] ceramic C-clamps. These clamps serve the dual purpose of lightly pressing the chip onto the fly-cut[18] surface of the copper block and securing electrical connections to the chip's gold contact pads. A press contact between the polished silicon chip and the fly-cut copper block ensures a good thermal contact between the chip and the stack so that as much heat may be dissipated by the stack as possible. The mechanical clamps are electrically insulating and thus allow for secure and reliable electrical connection to the chip. These connections

[17]Macor is a machinable, vacuum safe ceramic.

[18]Fly-cutting is a machining technique which can produce far flatter surfaces than conventional milling.

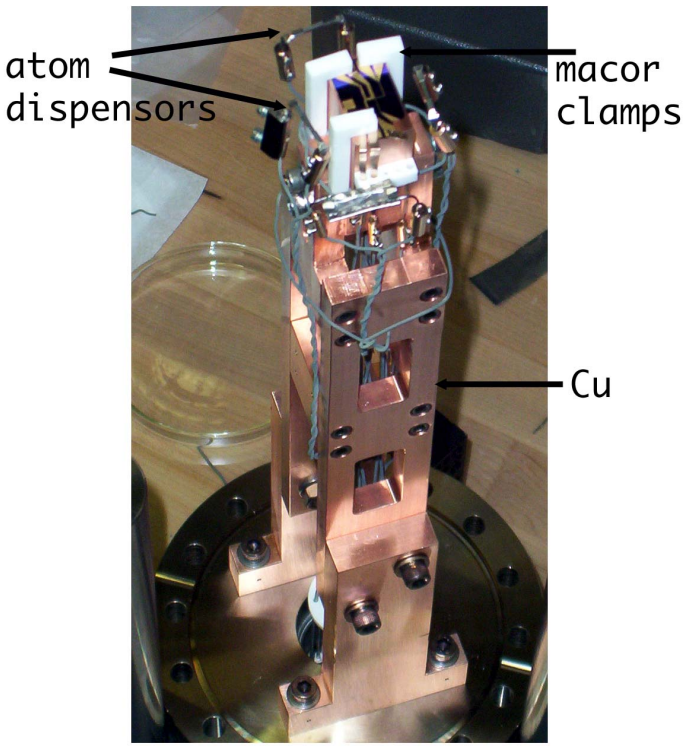

Figure 11: This photograph shows the full, completed stack just before insertion into the vacuum chamber. The body is copper and is attached to the vacuum side of a 6" UHV flange. Electrical connections are made with ceramic coated wire and the chip is attached to the very top by means of ceramic clamps (white). Note: the stack in inserted into the vacuum chamber chip-side down; the chip surface faces the $-z$ direction.

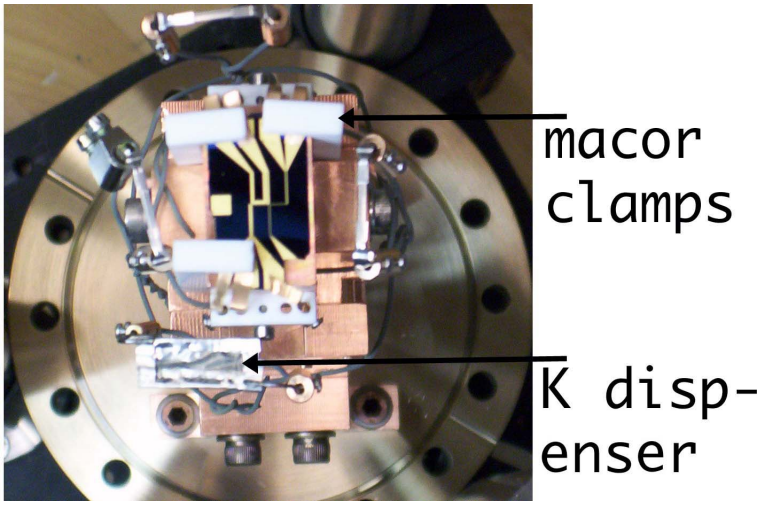

Figure 12: This photograph shows the stack in a top view. The chip is clamped to the surface of the Cu block with white macor clamps. The atom dispensers are mounted just away from the chip surface.

consist of thin beryllium-copper foil strips which are held in place by the macor clamps.

4.3 Electrical connections

Electrical signals are brought into the vacuum chamber through a vacuum electrical feedthrough. Ceramic coated wire[19] carries the current to the BeCu strips, and from there through the chip wires and back out of the vacuum system. Since conventional solder is a poor UHV material (due to excessive outgassing of the constituent Zn and Sn) all wire connections are made with BeCu crimp connectors and/or barrel connectors.

[19]The ceramic coating on bare copper wire is a vacuum compatible wire insulation.

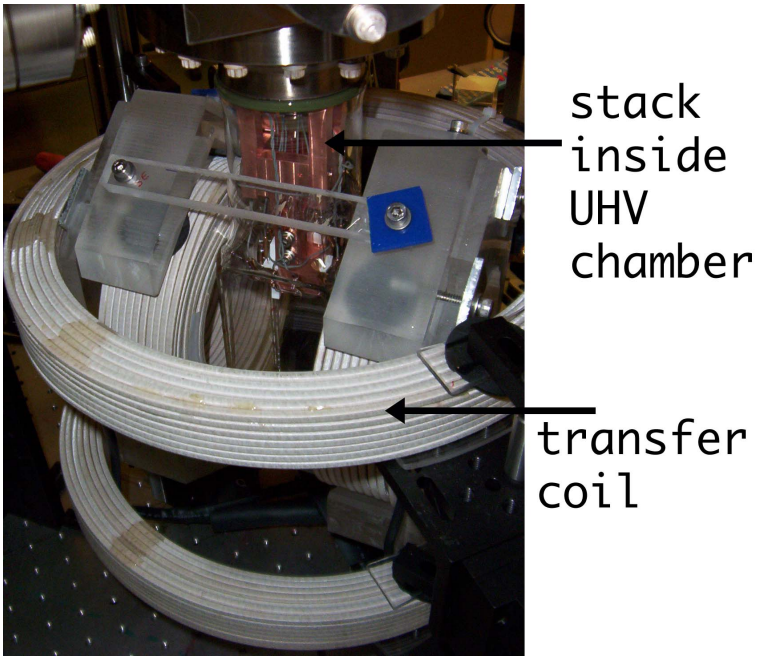

Figure 13: The stack mounted inside the vacuum chamber. Also visible are the MOT and transfer coils.

4.4 Atomic dispensers

The stack also serves as a scaffold from which to suspend the atomic sources. These dispensers are commercially bought SAES getters for ^{87}Rb or home-made getters for ^{40}K and are wired to the electrical feedthrough with ceramic-coated wire and crimp and/or barrel connectors. The dispensers are positioned just below the surface of the chip and are held in place by thin support wires which lash them to the sides of the stack.

5 Next steps

With the MOT and magnetic trap in place and the stack and chip mounted in the vacuum system our group is ready to make the final push toward

achieving quantum degenerate gases. Figure 14 is a schematic diagram of our progress to date and the relevance of my MSc. work this year to the overall project.

In the coming months I will be helping to perfect our techniques for transferring atoms from one trap to the next and to evaporatively cool first ^{87}Rb then ^{40}K atoms into quantum degeneracy.

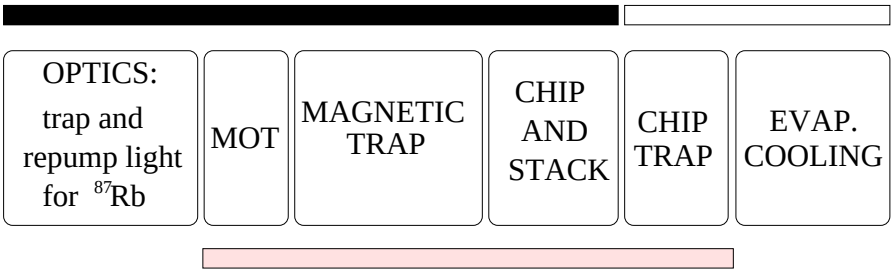

Figure 14: Major stages of our work toward achieving ultra-cold, quantum degenerate atoms. The upper bar indicates which tasks have been completed (black) and which have yet to be addressed (white). The lower bar spans those parts of the project to which my work is relevant.

Beyond Bose-Einstein condensation in ^{87}Rb, there is still the task of reaching Fermi degeneracy in ^{40}K. Our existing traps are suited to handle both atomic species, save for the cooling optics for ^{40}K, which have yet to be developed. I hope to contribute to our effort on this front as well as we approach our goal of carrying out experiments on trapped quantum degenerate fermionic atoms.

References

[1] M. H. Anderson, J. R. Ensher, M. R. Matthews, C. E. Wieman, E. A. Cornell, Observation of Bose-Einstein condensation in a dilute atomic vapor *Science* **269** 198-201 (1995).

[2] K. B. Davis, M.-O. Mewes, M. R. Andrews, N. J. van Druten, D. S. Durfee, D. M. Kurn, W. Ketterle, Bose-Einstein condensation in a gas of sodium atoms *Phys. Rev. Lett.* **75**, 3969-3973 (1995).

[3] C. A. Sackett, C. C. Bradley, M. Welling, R. G. Hulet, Bose-Einstein condensation of lithium, *Appl. Phys. B* **B65**, 433-440 (1997).

[4] B. deMarco, D. S. Jin, Onset of Fermi degeneracy in a trapped atomic gas, *Science* **285**, 1703-1706 (1999).

[5] D. Jaksch, C. Gruder, J.I. Cirac, C. W. Gardiner, P. Zoller, Cold bosonic atoms in optical lattices, *Phys. Rev. Lett.* **81**, 3108-3111 (1998).

[6] M. Greiner, O. Mandel, T.W. Hänsch, I. Bloch, Collapse and revival of the matter wave field of a Bose-Einstein condensate, *Nature*, **419**, 51-54, (2002).

[7] M. Greiner, O. Mandel, T. Esslinger, T.W. Hänsch, I. Bloch, Quantum phase transition from a superfluid to a Mott insulator in a gas of ultracold atoms, *Nature*, **415**, 39-44, (2002).

[8] S. Sachdev, *Quantum Phase Transitions*, Cambridge Univ. Press, Cambridge, 2001.

[9] C.A. Regal, M. Greiner, D. S. Jin, Observation of resonance condensation of Fermionic atom pairs, *Phys. Rev. Lett.*, **92**, 040403 (2004).

[10] Y. Ohashi, A. Griffin, BCS-BEC crossover in a trapped gas of Fermi atoms with a Feshbach resonance, *Physica B*, **329-333**, 40-41 (2003).

[11] C.A. Regal, D. S. Jin, Measurement of positive and negative scattering lengths in a Fermi gas of atoms, *Phys. Rev. Lett.*, **90**, 230404 (2003).

[12] M. Bartenstein, A. Altmeyer, S. Riedl, S. Jochim, C. Chin, J. H. Denschlag, R. Grimm, Crossover from a molecular Bose-Einstein condensate to a degenerate Fermi gas, *Phys. Rev. Lett.*, **92**, 120401 (2004).

[13] T. Bourdel, L. Khaykovich, J. Cubizolles, J. Zhang, F. Chevy, M. Teichmann, L. Tarruell, S. J. J. M. F. Kokkelmans, C. Salomon, Experimental study of the BEC-BCS crossover in lithium 6, *Phys. Rev. Lett.*, **93**, 050401 (2004).

[14] M. W. Zwierlein, C. A. Stan, C. H. Schunck, S. M. F. Raupach, A. J. Kerman, W. Ketterle, Condensation of pairs of fermionic atoms near a Feshbach resonance, *Phys. Rev. Lett.*, **92**, 100401 (2004).

[15] W. Hofstetter, J. I. Cirac, P. Zoller, E. Demler, M. Lukin, High-temperature superfluidity of fermionic atoms in optical lattices, *Phys. Rev. Lett.*, **89**, 220407 (2002).

[16] H. J. Metcalf, P. van der Straten, *Laser Cooling and Trapping*, Springer-Verlag New York, Inc., New York, 1999.

[17] W. H. Wing, *Prog. Quantum Electron.*, **8**, 181 (1984).

[18] J. Reichel, Microchip traps and Bose-Einstein condensation, *Appl. Phys. B*, **75**, 469-487 (2002).

[19] W. Hänsel, J. Reichel, P. Hommelhoff, T. W. Hänsch, Magnetic Conveyor Belt for Transporting and Merging Trapped Atom Clouds, *Phys. Rev. Lett.*, **86**, 608-611 (2001).

[20] W. R. Smythe, "Static and dynamic electricity", p.290, McGraw-Hill, 1968.

[21] T. Bergeman, G. Erez, H. Metcalf, Magnetostatic trapping fields for neutral atoms, *Phys. Rev. A*, **35**, 1535-1546 (1987).

[22] V. Vuletic. Lecture notes from the 2004 Boulder Summer School for Condensed Matter and Materials Physics, Boulder, CO, July 2004.

[23] J. D. Weinstein and K. G. Libbrecht, Microstopic magnetic traps for neutral atoms, *Phys. Rev. A*, **52**, 4004-4009 (1995).

[24] J. Reichel, W. Hänsel, P. Hommelhoff, T. W. Hänsch, Applications of integrated magnetic microtraps, *Appl. Phys. B*, **72**, 81-89 (2001).